

OXIDATION CHARACTERISTICS OF THE SEMICOKE FROM THE RETORTING OF OIL SHALE AND WHEAT STRAW BLENDS IN DIFFERENT ATMOSPHERES

MAO MU, XIANGXIN HAN*, BIN CHEN, XIUMIN JIANG

Institute of Thermal Energy Engineering, School of Mechanical Engineering, Shanghai Jiao Tong University, Shanghai 200240, People's Republic of China

Abstract. *A new way of utilizing oil shale is its co-retorting with wheat straw for oil. However, the process generates a great amount of combustible solid semicoke waste. To utilize this waste effectively for heating the retorting process, the current work investigated its oxidation characteristics by employing a combined thermogravimetry-mass spectrometry (TG-MS) system, and discussed the effects of three parameters, including the wheat straw mass fraction of matrix samples, as well as different ambient gases and their O₂ volume fraction, on the oxidation of the semicoke. In the presence of O₂, the whole oxidation process of semicoke samples mainly consists of two stages: the combustion stage (300–600 °C) in which water, CO, CO₂ and pollutants are mainly released, and the decomposition stage (600–1000 °C) in which carbonates and sulphates decompose to release CO₂ and SO₂, respectively. In the combustion stage, increasing both the wheat straw proportion of the original sample and the O₂ volume fraction can improve the combustion performance of the resulting semicoke blends. In the decomposition stage, the gasification reaction also occurs to produce CO. During the entire oxidation process, semicoke in 21% O₂/79% CO₂ would give off less NO_x and SO₂ than in air. And, SO₂ formation is also influenced by the O₂ fraction, especially above 900 °C.*

Keywords: *thermogravimetry-mass spectrometry, oil shale retorting, wheat straw, semicoke, oxidation.*

1. Introduction

With the economic growth and ever-expanding urbanization, there is an increasing demand for energy in China. But as traditional fossil fuels such as coal, crude oil and natural gas are depleting, alternative fuels have attracted more and more attention in recent times. Being one of the most important

* Corresponding author: e-mail hanxiangxin@sjtu.edu.cn

substitutes for crude oil, oil shale has widely been studied to find its most cost-effective and environmentally friendly utilization process.

As one of alternative fuels, biomass has aroused considerable concern as its utilization could lead to zero net CO₂ emissions, if taking both the photosynthesis process and the application process into consideration. In China, the potential yield of biomass is equal to 7,960 million tons of standard coal, 24.6% of which are plants straw [1]. There are many ways of using biomass as fuel, such as direct combustion, gasification, liquefaction and biological conversion. However, in the rural areas of China, biomass is often directly combusted, which causes environmental problems. Therefore, it is of great significance to find effective technologies to utilize biomass. Pyrolysis, one of the modes of liquefaction, suits well for this purpose, being cost-effective and producing high-oxygen oil. The latter, in turn, should be further refined to be used as a substitute for crude oil [2]. So, many researchers have pyrolyzed biomass with waste plastics, tires, coal, etc., and found that co-pyrolysis could increase the yield of the obtained oil and upgrade its quality [2–5]. Recently, the authors of this work investigated the co-retorting of oil shale and wheat straw [6]. It was found that the H free radical from the decomposition of wheat straw could induce the cracking of the bridge bonds of kerogen and accelerate the pyrolysis reaction. Furthermore, the obtained oil contained more saturated hydrocarbons and had a high H/C ratio, which is beneficial to the further upgrading of the pyrolytic oil. However, the co-retorting of oil shale and wheat straw brings about a new issue of how to deal with semicoke as a by-product. The most popular commercial oil shale retorts, Kiviter and Fushun, employ internal combustion technology and feature high thermal efficiency. The semicoke in these processes drops down from the upper retort section, smolders and releases energy in the ascending current of air-steam. The resulting hot flue gas enters the upper retort section, heats oil shale and brings gas products out of the retort section. Since the excess air from the bottom will burn out a portion of oil in the retort section, the oil yield is usually lower than 80% of Fischer assay's. In the actual operation, these two processes cannot consume all the combustible material in the oil shale semicoke, which leads to semicoke waste. In addition, the fuel gas from the retorts has a low heating value due to its high content of N₂. To overcome these problems, the authors suggested that the air directed into the lower part of the retort should be replaced by the mixture of O₂ and CO₂. This is first because unlike N₂, CO₂ can react with semicoke, reducing its combustible material content. Secondly, the O₂ concentration of the mix gas can be adjusted below the 21% of air, which slows down the oxidation of shale oil. The third reason is that CO₂ in ambient gas generates a reductive atmosphere and thus reduces NO_x emission [7]. And, last, the ambient gas containing a high concentration of CO₂ could promote the sulphuration of KCl in wheat straw semicoke and alleviate the high-temperature corrosion [8]. In addition, researches on co-

combustion of biomass and fuels other than oil shale have shown that minerals in the ash of biomass could abate SO₂ emission [9–13].

Given all the considerations above, it would be beneficial to burn semicoke in a high-concentration CO₂ atmosphere. Therefore, it is necessary to investigate the fundamental oxidation characteristics of semicoke in O₂/CO₂ atmosphere. According to many researches [9, 11, 14–16], a coupled system consisting of a thermogravimetric (TG) analyzer and a mass spectrometry (MS) analyzer is a simple but reliable tool for exploring the fundamental characteristics of fuels. Thus, by use of thermogravimetry-mass spectrometry (TG-MS), this work compares the oxidation processes of samples in O₂/CO₂ atmosphere and air, as well as discusses the effects of the wheat straw fraction in original samples and the O₂ fraction in the carrier gas (O₂/CO₂) on the oxidation process. The results provide useful information about the combustion performance and pollutants emission trend of semicoke samples.

2. Experimental

2.1. Sample preparation

The oil shale sample used in this work was obtained from Dachengzi mine located in Huadian city, China, and the wheat straw sample was collected from Northeast China. The semicokes of oil shale and wheat straw were prepared as follows. Firstly, oil shale lumps were cracked and sieved and the wheat straw sample was ground, to obtain particles of both less than 3 mm in size. Then the oil shale and wheat straw samples were prepared by mixing the components at five mass ratios – 1:0, 3:1, 1:1, 1:3 and 0:1. Thereafter each sample was subjected to retorting in a fixed bed retort system from room temperature to the final temperature of 520 °C at an average heating rate of 10 °C/min, and maintained at 520 °C for 20 minutes. During the heating, argon as a purge gas flowed through the system at a flow rate of 0.3 L/min. The experiments with each sample were performed at least twice. Finally, the semicoke samples obtained from the retorting were marked as S_{1–5}, respectively, according to the mass ratios of the matrix oil shale and wheat straw, and then ground below 0.2 mm for TG-MS experiments.

Table 1 presents the results of proximate and ultimate analyses of semicoke samples; the compositional data about their raw material have been given by Chen et al. [6]. The researchers established that there occurred interactions between samples of raw wheat straw and oil shale during the retorting. As a result, the lower heating values as well as fixed carbon contents of the samples varied. Moreover, the volatile content in semicoke samples decreased with increasing mass ratio of wheat straw in matrix samples. This indicates that the semicoke samples exhibited different combustion behaviors, which will be discussed in the following parts. In addition, all semicoke samples had a similar ash content.

Table 1. Proximate and ultimate analyses of semicoke samples

Sample	Sample		Low heat value, kJ/kg	Ultimate analysis, %				Proximate analysis, %			
	x_O	x_{WS}		N	C	H	S	M _{ad}	A _{ad}	FC _{ad}	V _{ad}
S ₁	1.00	0	4902.84	0.64	16.82	1.03	0.88	1.50	72.62	7.75	18.12
S ₂	0.73	0.27	5455.09	0.61	17.57	0.96	0.76	1.70	72.66	9.86	15.78
S ₃	0.48	0.52	5834.74	0.55	18.19	0.96	0.57	1.69	72.26	12.14	13.90
S ₄	0.24	0.76	6164.30	0.49	18.00	0.88	0.41	1.05	72.42	13.01	13.51
S ₅	0	1.00	5722.62	0.41	16.25	0.75	0.23	1.15	74.31	12.70	11.84

M – moisture, A – ash, FC – fixed carbon, V – volatiles; ad – air-dry basis; x_O and x_{WS} are the calculated mass fractions of oil shale semicoke and wheat straw semicoke, respectively.

2.2. TG-MS experiments

TG-MS experiments were performed using a Mettler-Toledo TGA/DSC/1600 TG analyzer and a Pfeiffer Vacuum D-35614 MS analyzer. Mixtures of O₂ and CO₂ containing respectively 0, 5, 10, 15 and 21% O₂, by volume, were used as carrier gases at a constant flow rate of 50 ml/min. TG-MS experiments with sample S₃ were conducted in the mixture of said gases and in air from room temperature to 1000 °C at a heating rate of 20 °C/min and maintained at 1000 °C for 5 minutes. In addition, each semicoke sample of about 10 mg was heated in the TG-MS system in the mixture of O₂ and CO₂ as the carrier gas containing 21% O₂. Also, a blank test (a crucible with no sample) was performed in the beginning of experiments.

The MS analyzer scanned the mass/charge ratio from 1 to 120 at 50 ms/per. The mass/charge ratios of 16 (CH₄), 17 (NH₃ or OH), 18 (H₂O), 26 (C₂H₂), 28 (CO or C₂H₄), 30 (NO or C₂H₆), 32 (O₂), 34 (H₂S), 42 (C₃H₆), 44 (CO₂ or C₃H₈), 46 (NO₂) and 64 (SO₂) indicated the main gas products from the combustion of semicoke samples. In addition, the main gas products with mass/charge ratios of 15 (CH₃), 27 (C₂H₃), 29 (C₂H₅), 41 (C₃H₅) and 43 (C₃H₇) were also identified, to find out whether there existed hydrocarbon gases. The peak areas of specified pollutant signals (NO, NO₂ and SO₂) were calculated and then divided by the initial sample mass to eliminate the effect of sample mass on signal intensity.

2.3. Measurement of combustion parameters

Previous research suggests that oil shale semicoke from the retorting at a temperature of 520 °C would ignite heterogeneously [17]. The whole oxidation process consists of the combustion stage (300–600 °C) and the decomposition stage (600–1000 °C). In the combustion stage, the ignition temperature (T_i , °C), burnout temperature (T_b , °C), peak temperature (T_{max} , °C) and other pertinent parameters could be obtained from TG and differential thermogravimetry (DTG) data [18]. In addition, the ignition index and the combustion index were also used to assess the combustion behavior of samples [19, 20]. The ignition index is defined as follows:

$$D = \frac{R_{\max}}{t_m t_i}, \quad (1)$$

where R_{\max} is the maximum mass loss rate, %/s; t_m is the time when the mass loss rate reaches R_{\max} , s; and t_i is the time during which the temperature arrives at T_i , s. The higher the ignition index is, the better the ignition performance is.

The combustion index is determined by Equation (2):

$$S = \frac{R_{\max} R_{\text{mean}}}{T_i^2 T_b}, \quad (2)$$

where R_{mean} is the mean mass loss rate, %/s. The higher the combustion index is, the better the combustion performance is.

2.4. Kinetic model

The kinetic model assumes the reaction rate (da/dt) to depend on two independent variables, temperature and mass loss fraction (α , %). a is determined as follows:

$$\alpha = \frac{W_0 - W}{W_0 - W_\infty}, \quad (3)$$

where W_0 , W and W_∞ are respectively the initial mass, the mass at any temperature, and the final mass, kg or mass%.

In this work, the reaction model applied was the n_{th} order reaction model. The reaction order (n), the pre-exponential factor (A , s^{-1}) and the activation energy (E , kJ/mol) were obtained using the Coats-Redfern integration method [21].

3. Results and discussion

3.1. TG and DTG analysis

3.1.1. TG and DTG of samples

Figures 1a and 1b show TG and DTG curves of semicoke heated in 21% O₂ and 79% CO₂ (21O₂/79CO₂). In the heating process from room temperature to 200 °C, there is a slight mass loss as a result of moisture evaporation. In the temperature range of 300–600 °C, volatiles are released and the combustible gas and solids burn quickly, leading to a sharp mass loss. So, this temperature range is called the combustion stage. Due to previous retorting, most of the organic matter in raw wheat straw and oil shale has converted into hydrocarbon gases and oil. So, the residual semicoke blends contain much less volatiles and have only one peak in the combustion

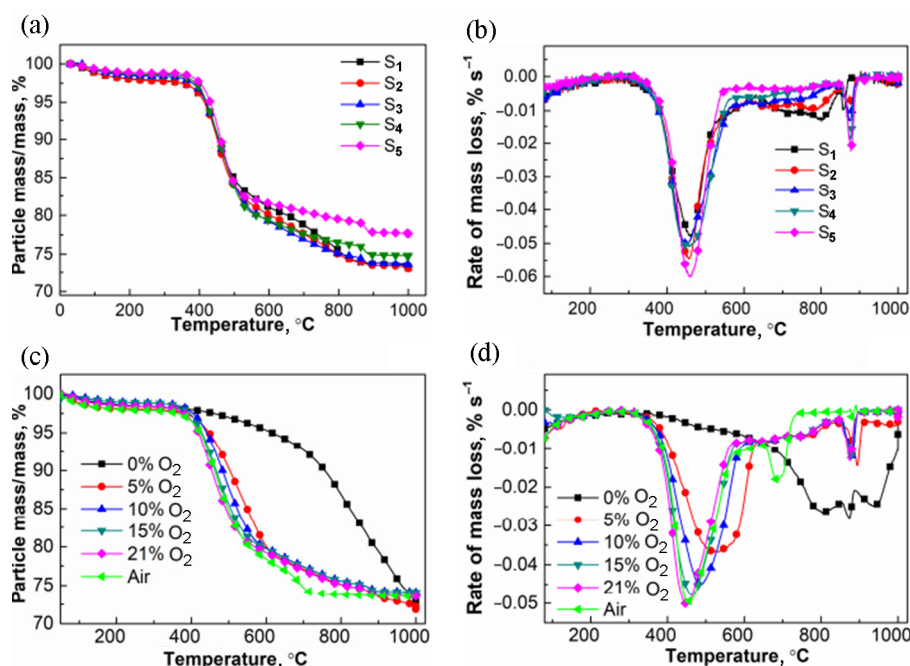


Fig. 1. TG and DTG curves of semicoke samples in different atmospheres: (a) TG curves of samples S₁–S₅ in 21% O₂ and 79% CO₂; (b) DTG curves of samples S₁–S₅ in 21% O₂ and 79% CO₂; (c) TG curves of sample S₃ in different atmospheres; (d) DTG curves of sample S₃ in different atmospheres.

process, unlike samples of other blends with no retorting pretreatment that have two major peaks [9, 10, 12, 22]. The second mass loss begins at 600 °C, but the mass loss rate is slower. This may mainly be attributed to the slow reactions of carbonates, accompanied with CO₂ emission. All semicoke samples lose mass and give off SO₂ as the temperature exceeds 900 °C, which will be discussed in the following parts. Therefore, the temperature range of 600–1000 °C is called the decomposition stage in this work. In general, all semicoke samples have both the combustion and decomposition stages in the 21O₂/79CO₂ atmosphere. However, there are also some notable differences in combustion behavior between the samples. For example, as seen from Table 2, sample S₅ has a maximum mass loss rate R_{\max} and the lowest burn-out temperature T_b , but its ignition temperature T_i is close to that of other samples. In addition, the second mass loss and its rate of sample S₅ are both lower than those of sample S₁.

Figures 1c and 1d show TG and DTG curves of sample S₃ in different atmospheres. In a pure CO₂ atmosphere, the main mass loss is attributed to the volatiles release in the low-temperature range (300–600 °C) and the char gasification, as well as the reaction of carbonates and the decomposition of sulphates in the high-temperature range (600–1000 °C). After O₂ appears and increases gradually, the shapes of TG and DTG curves change, showing

that the oxygen concentration of the carrier gas indeed has an effect on the combustion characteristics of semicoke, such as T_{\max} and R_{\max} . Calculated from TG and DTG curves, the temperature T_{\max} corresponding to the maximum mass loss rate decreases obviously with increasing O_2 content from 5 to 21%; by contrast, the maximum mass loss rate R_{\max} increases. These results indicate that a higher oxygen concentration leads to higher reaction rates and a shorter reaction time. Therefore, the semicoke samples heated in an atmosphere of 5%, 10% and 15% O_2 still undergo reaction in the temperature range of 560–600 °C, while in the atmosphere of 21% O_2 the sample mass almost does not change, as Figures 1c and 1d show. Furthermore, both T_{\max} and R_{\max} in 21% O_2 /79% CO_2 are close to those in air, but the decomposition of carbonates in air is more intense.

Table 2 and Table 3 reveal the variations of the ignition and combustion indexes of different semicoke samples. It can be seen that the wheat straw semicoke sample S_5 has higher ignition and combustion indexes compared with the oil shale semicoke sample S_1 . Also, as Table 3 displays, the said indexes of sample S_3 increase gradually when the O_2 concentration in the carrier gas rises from 5 to 21%, which agrees with the finding of Vamvuka

Table 2. Combustion characteristics of semicoke samples in 21% O_2 and 79% CO_2

Sample	R_{\max} , %/s	T_{\max} , °C	T_i , °C	t_i , s	t_b , s	T_b , °C	D	S
S_1	-0.0477856	460.67	403.46	1120.39	1607.49	565.83	3.32	1.48
S_2	-0.0544887	456.00	405.54	1126.61	1559.78	549.93	3.79	1.99
S_3	-0.0506538	450.00	399.65	1108.95	1590.91	560.30	3.63	1.93
S_4	-0.0509741	456.33	399.30	1107.91	1572.35	554.12	3.60	2.08
S_5	-0.0601664	461.33	412.64	1147.93	1495.36	528.45	4.05	2.76

R_{\max} – maximum mass loss rate; T_{\max} – temperature corresponding to maximum mass loss rate;

T_i – ignition temperature; t_i – ignition time; t_b – burn-out time; T_b – burn-out temperature;

D – ignition index, $10^{-10}*(\%*s^{-3})$; S – combustion index, $10^{-15}*(\%^2*s^{-2}*(^{\circ}C)^{-3})$.

Table 3. Combustion and pyrolysis characteristics of sample S_3 in different atmospheres

Atmosphere	R_{\max} , %/s	T_{\max} , °C	T_i , °C	t_i , s	t_b , s	T_b , °C	D	S
0% O_2	-0.000283	872.00	–	–	–	–	–	–
5% O_2	-0.000385	515.67	441.43	1234.30	1895.65	661.88	2.03	0.78
10% O_2	-0.000451	488.67	420.33	1170.98	1703.59	597.86	2.80	1.35
15% O_2	-0.000480	464.33	407.38	1132.14	1632.74	574.25	3.25	1.66
21% O_2	-0.000507	450.00	401.47	1114.40	1589.60	559.87	3.61	1.92
Air	-0.000505	460.67	404.25	1122.76	1592.42	560.81	3.53	1.92

R_{\max} – maximum mass loss rate; T_{\max} – temperature corresponding to maximum mass loss rate;

T_i – ignition temperature; t_i – ignition time; t_b – burn-out time; T_b – burn-out temperature;

D – ignition index, $10^{-10}*(\%*s^{-3})$; S – combustion index, $10^{-15}*(\%^2*s^{-2}*(^{\circ}C)^{-3})$; “–” represents no data.

et al. [23]. Consequently, the ignition and combustion indexes of semicoke blends exhibit an increasing trend with the increase of the wheat straw content of the sample and the O₂ fraction in the carrier gas.

3.1.2. Synergetic effect on semicoke blends during the combustion

It deserves to be studied more thoroughly whether there is a synergetic effect on semicoke blends during the combustion. To determine the theoretical normalized mass of the blends depending on the experimental normalized mass of an individual semicoke sample, the following equations were employed:

$$M_{exp} = W/W_0, \quad (4)$$

$$M_{cal} = x_o M_o + x_{ws} M_{ws} \quad (5)$$

where M_{exp} is the normalized mass of experimental sample, M_o and M_{ws} represent the normalized masses of pure oil shale semicoke and pure wheat straw semicoke at the same moment, respectively, and x_o and x_{ws} are the proportions of oil shale semicoke and wheat straw semicoke in the mixture, respectively. The two calculated ratios are listed in Table 1. Figure 2a shows comparatively theoretical and experimental TG curves of semicoke blends. The discrepancies between the curves help distinguish the synergetic effect, calculated on the basis of the following equation (Fig. 2b):

$$Discrepancy(\%) = -\frac{(M_{exp} - M_{cal})}{M_{exp}} \times 100. \quad (6)$$

As seen from Figure 2, the theoretical and experimental TG curves of the blends below 400 °C are almost similar since there is no ignition of samples at this temperature. But above 400 °C, due to the occurrence of combustion

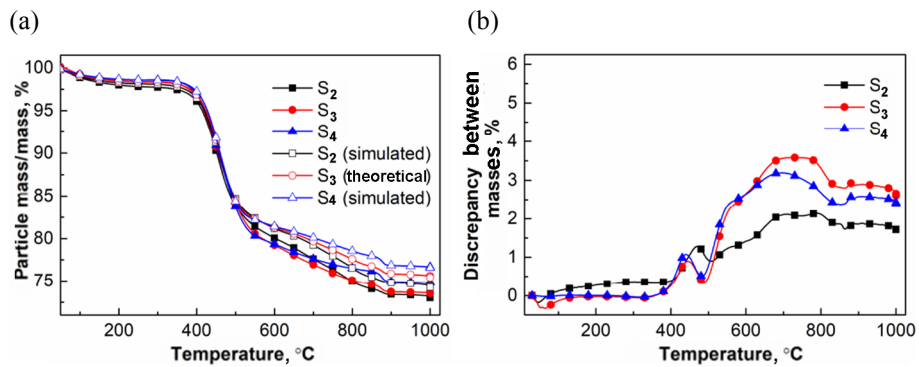


Fig. 2. Mass loss of semicoke samples and discrepancy between theoretical and experiment in 21% O₂: (a) experimental and theoretical TG curves of samples S₂–S₄; (b) discrepancy between masses of samples S₂–S₄.

and decomposition reactions, the curves exhibit dissimilarities. The maximum discrepancy between the TG curves is 3.5%, which, however, does not exceed the statistical significance, 5% [13]. This is indicative of the absence of the synergetic effect on semicoke blends in the two stages, combustion and decomposition.

3.1.3. Kinetic analysis

TG and DTG curves show that the whole oxidation process consists of two stages. Thus, the kinetic parameters of each stage were calculated individually by applying the Coats-Redfern equation. The reaction order, n , increased progressively from 1.0 to 2.0 at a step of 0.1. Finally, the reaction order corresponding to the maximum correlation coefficient between the fitting straight line and calculated results was determined as the most suitable one. Then, after the fitting line was determined, the activation energy E and the pre-exponential factor A could be obtained one by one from the line slope, as a function of E , and its intercept, as a function of E and A . The fierce exothermic effect of the materials would make the kinetic data (α vs T) unreliable to calculate the activation energy, according to Vyazovkin et al. [24]. Therefore, the difference between the sample temperature (T_s) and the oven temperature or reference temperature (T_r) should be taken into account. Similarly, the standard deviation of activation energy calculated on the basis of kinetic data α vs T_s and α vs T_r has to be considered. In this work, the standard deviation between the two calculated activation energies was under 5%, indicating that the results were reliable.

Table 4 presents the activation energy of different semicoke samples in the mixture of 21% O₂ and 79% CO₂. Generally speaking, increasing the wheat straw fraction in original samples elevates the E of their semicoke blends in the combustion stage. That is, the higher the proportion of wheat straw in the matrix mixture sample is, the lower the amount of volatiles in the resulting semicoke is and the more difficultly the semicoke sample

Table 4. Kinetic analysis of different samples in 21% O₂ and 79% CO₂

Sample	Temperature range, °C	A , s ⁻¹	E , kJ/mol	n	r	S/ E' , %
S ₁	300–600	9.97E + 07	119.39	1.6	0.99	2.35
	600–1000	1.74E + 08	169.35	2	0.98	0.30
S ₂	300–600	3.18E + 08	126.19	1.6	0.99	1.95
	600–1000	2.14E + 07	151.93	1.8	0.98	0.54
S ₃	300–600	1.43E + 09	135.09	1.7	0.99	2.62
	600–1000	4.04E + 06	138.80	1.6	0.97	0.38
S ₄	300–600	1.10E + 10	146.96	1.7	0.99	4.34
	600–1000	2.88E + 05	119.74	1.4	0.95	0.20
S ₅	300–600	1.17E + 11	160.36	1.7	1.00	2.67
	600–1000	2.91E + 05	120.79	1.3	0.96	1.20

S – standard deviation; E' – average activated energy.

ignites. But, once ignited, the semicoke resulting from the retorting of the matrix mixture containing wheat straw (samples S₂–S₅) burns more quickly and stably than oil shale semicoke (sample S₁), as judged by the ignition and combustion indexes.

Table 5 reveals the variation of the activation energy of sample S₃ in different atmospheres. The E of the first mass loss stage in a pure CO₂ atmosphere is 65.46 kJ/mol, which is smaller than the respective figure in oxidic conditions. With the O₂ content increasing from 5 to 21%, the activation energy of the first combustion stage also goes up. This may be attributed to that more and more residual carbon in sample S₃ is involved in the first combustion reaction stage, consuming more energy than the pyrolysis reaction. Besides, the E of the first combustion stage in air is smaller than that in 21O₂/79CO₂ since O₂ has a lower diffusion rate in 21O₂/79CO₂ than in air [25].

Table 5. Kinetic analysis of sample S₃ in different atmospheres

Atmosphere	Temperature range, °C	A , s ⁻¹	E , kJ/mol	n	r	S/E' , %
0% O ₂	300–600	4.17E + 03	65.46	1.0	0.98	2.52
	600–1000	1.55E + 05	125.56	1.3	0.97	0.88
5% O ₂	300–650	6.34E + 07	122.21	2.0	0.99	0.07
	650–1000	3.85E + 05	129.12	1.6	0.94	1.35
10% O ₂	300–600	8.01E + 07	122.25	1.4	0.99	0.75
	600–1000	3.32E + 06	137.22	1.6	0.96	1.00
15% O ₂	300–600	4.47E + 08	129.56	1.6	0.99	0.39
	600–1000	3.94E + 06	138.55	1.6	0.96	1.05
21% O ₂	300–600	1.43E + 09	135.09	1.7	0.99	2.62
	600–1000	4.04E + 06	138.80	1.6	0.97	0.38
Air	300–600	3.44E + 08	127.31	1.6	0.99	0.01
	600–1000	3.40E + 08	161.13	2.0	0.94	0.57

S – standard deviation; E' – average activated energy.

3.2. Mass spectrometry

3.2.1. Effect of the wheat straw mass fraction on the gas evolved

Figures 3–5 illustrate the MS analysis of the main gaseous products from TG experiments of semicoke, including hydrocarbons, NO_x, SO₂, CO, etc. Figure 3 shows the history of evolution of several gaseous products from the oxidation of different semicoke samples in 21O₂/79CO₂. In the combustion stage (300–600 °C), CO, CO₂ and H₂O reach their peak values near 450 °C, which is attributed to the combustion reactions of combustibles. In addition, the curves of CO₂ still have small peaks above 600 °C due to both the direct sulphuration and decomposition of carbonates, as Reactions (7) and (8) show. At the same time, the CO curves have peaks above 600 °C, which is mainly attributed to Reaction (9):





From Figure 4 it can be seen that the release of hydrocarbon gases mainly takes place in the temperature range of 300–600 °C, as a result of the devolatilization and incomplete combustion of organic matter. The temperature corresponding to the maximum gas release peak is also close to 450 °C. H₂S (m/z = 34) does not show peaks during the whole oxidation process under conditions with different oxygen concentrations. The absence of H₂S may be ascribed to the oxidation of H₂S into SO₂. Figure 4 reveals

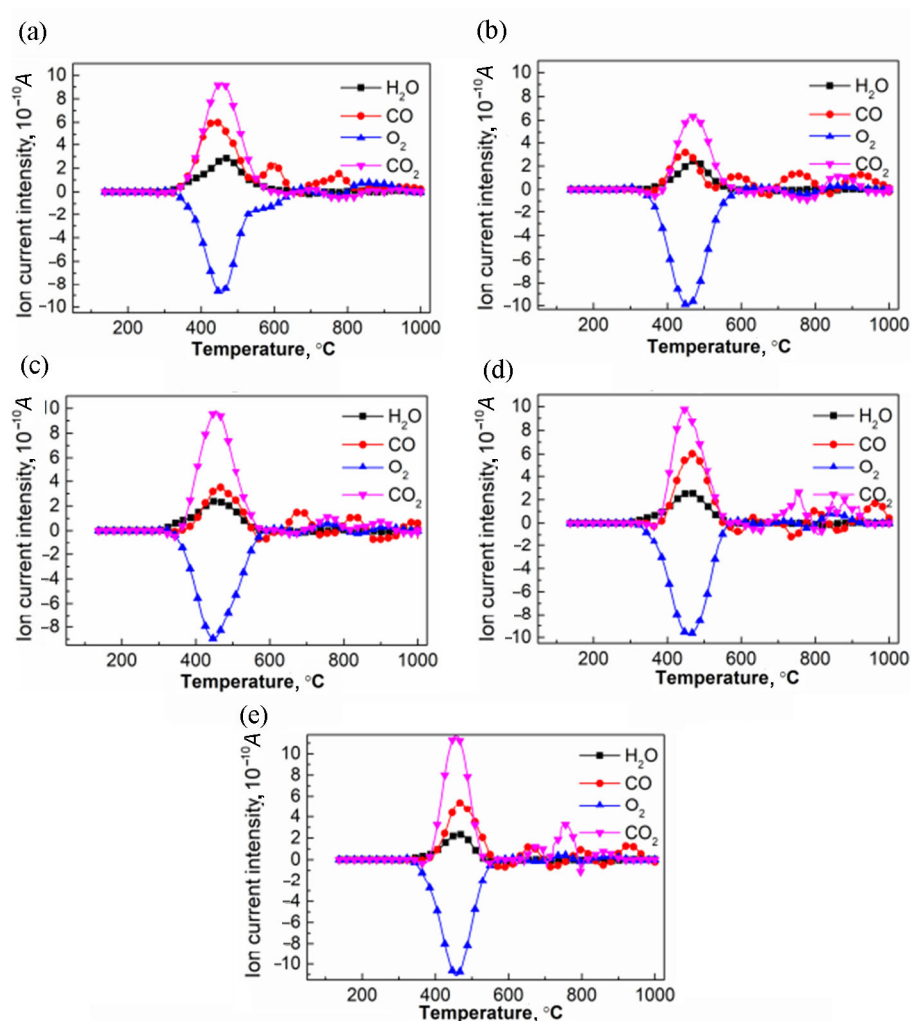


Fig. 3. Products evolution from combustion of different samples in 21% O₂ and 79% CO₂: (a) sample S₁; (b) sample S₂; (c) sample S₃; (d) sample S₄; (e) sample S₅.

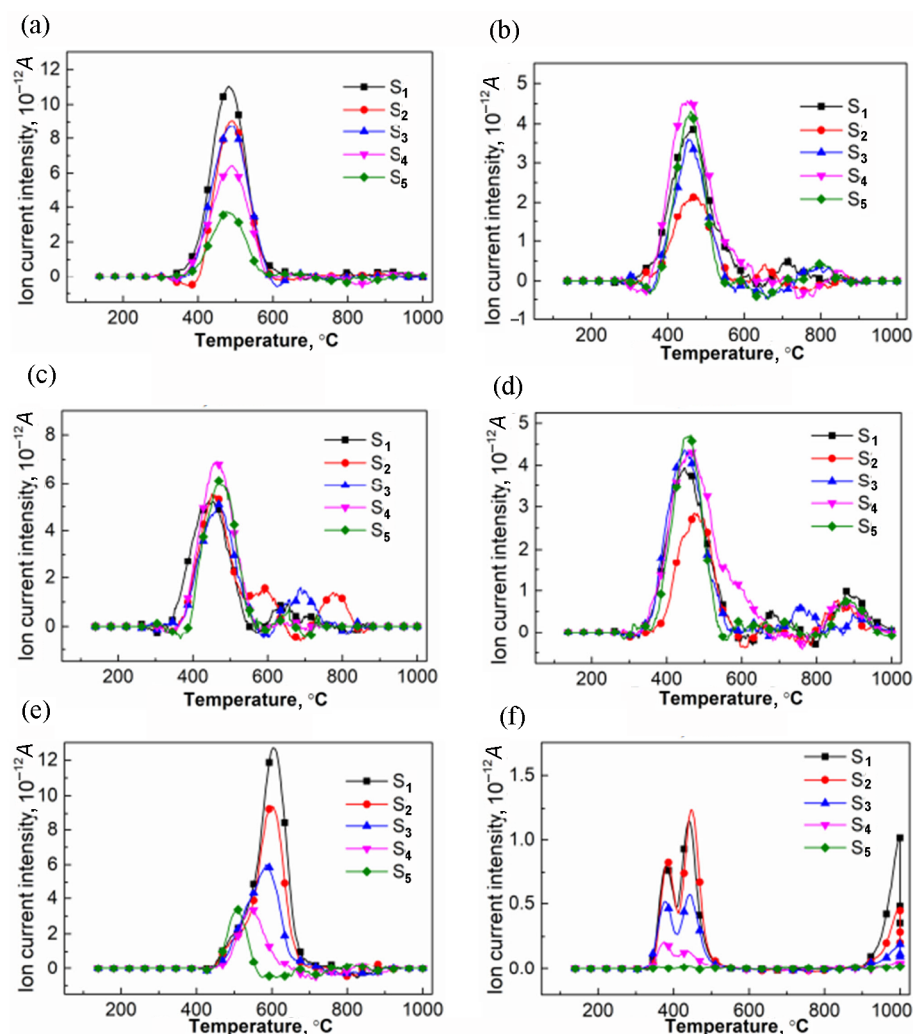


Fig. 4. Evolution of hydrocarbon gas and pollutants from combustion of different samples in 21% O₂ and 79% CO₂: (a) C₂H₃; (b) C₃H₇; (c) C₂H₅; (d) NO₂; (e) NO; (f) SO₂.

that, with the exception of sample S₅ whose SO₂ curve is at zero, those of other samples have peaks in the temperature range of 300–650 °C. Above 900 °C, all samples show SO₂ emission peaks, due to the decomposition of sulphates in ash [26]. $m/z = 29$ (Fig. 4c) and $m/z = 30$ (Fig. 4e) give evidence of the presence of C₂H₆ and NO, of which C₂H₆ can be broken into C₂H₅ ($m/z = 29$) by the MS system, and therefore, $m/z = 30$ represents NO. It is evident that both the emission and the peak temperature of NO decrease with increasing wheat straw fraction of the original sample. And, increasing the wheat straw fraction in original samples also decreases the emission of

SO₂ from semicoke samples, as Figure 4f displays, even though in the combustion stage (300–600 °C), the SO₂ emission from sample S₂ is very close to that from sample S₁ in the same stage. In general, if the sum of NO and NO₂ is regarded as NO_x, both NO_x and SO₂ emissions from semicoke combustion decrease with increasing wheat straw proportion in original samples because this increase leads to the decline of sulphur and nitrogen contents in the semicoke.

3.2.2. Effect of atmosphere on the gas evolved

Figures 5 and 6 illustrate the evolution of gaseous products of sample S₃ in different atmospheres. In a pure CO₂ atmosphere, CO is formed mainly in the temperature range of 700–1000 °C, later than under oxic conditions (Fig. 5). Meanwhile, the release of CO is always accompanied with the decrease of CO₂, which further proves that CO₂ reacted with carbon to form CO. Besides, if O₂ is present, H₂O, CO and CO₂ evolve earlier, in the temperature region of 300–600 °C, which is always accompanied with an abrupt decrease of O₂. Furthermore, the temperatures corresponding to the peaks of curves of CO, CO₂ and H₂O decrease with increasing oxygen concentration.

Figure 6 shows that, unlike CO, hydrocarbon gas is released more gently in a pure CO₂ atmosphere than in an oxygen-bearing atmosphere. Figure 6 also plots the pollutant emissions of sample S₃ in different atmospheres. In the pure CO₂ atmosphere, the emission of NO and NO₂, resulting from the collision of nitrogen-containing species or radicals with oxygen-bearing species or radicals in the semicoke [27], is more intense as the temperature rises. When O₂ is present, higher quantities of NO and NO₂ are released during the combustion reactions of semicoke at 300–600 °C. No matter what the O₂ concentration is, SO₂ always shows peaks in two temperature ranges: 350–600 °C and 900–1000 °C. In the combustion stage (300–600 °C), the SO₂ emission results from the decomposition (in a pure CO₂) or combustion (in 5–21% O₂) reactions of organic sulphur and pyrite [28]. At 900–1000 °C, the peak of SO₂ is ascribed to the decomposition of sulphates in ash. Researches have indicated that the sulphates would decompose to SO₂ or SO₃. But in our experiments, there was no obvious change of SO₃ curves. So, the decomposition mechanism can be described as follows:



Figure 6 also demonstrates that the peak area of NO decreases with O₂ increasing from 5 to 21%, while that of NO₂ is increased. As a result, increasing O₂ in the carrier gas has only a little influence on total NO_x emission because this converts more NO into NO₂ through Reaction (11). And, what is more important, the NO_x emission in 21O₂/79CO₂ is less intense than that in air. So is the SO₂ emission. This is consistent with the findings of other researches [13, 29–31] and is ascribed to the direct

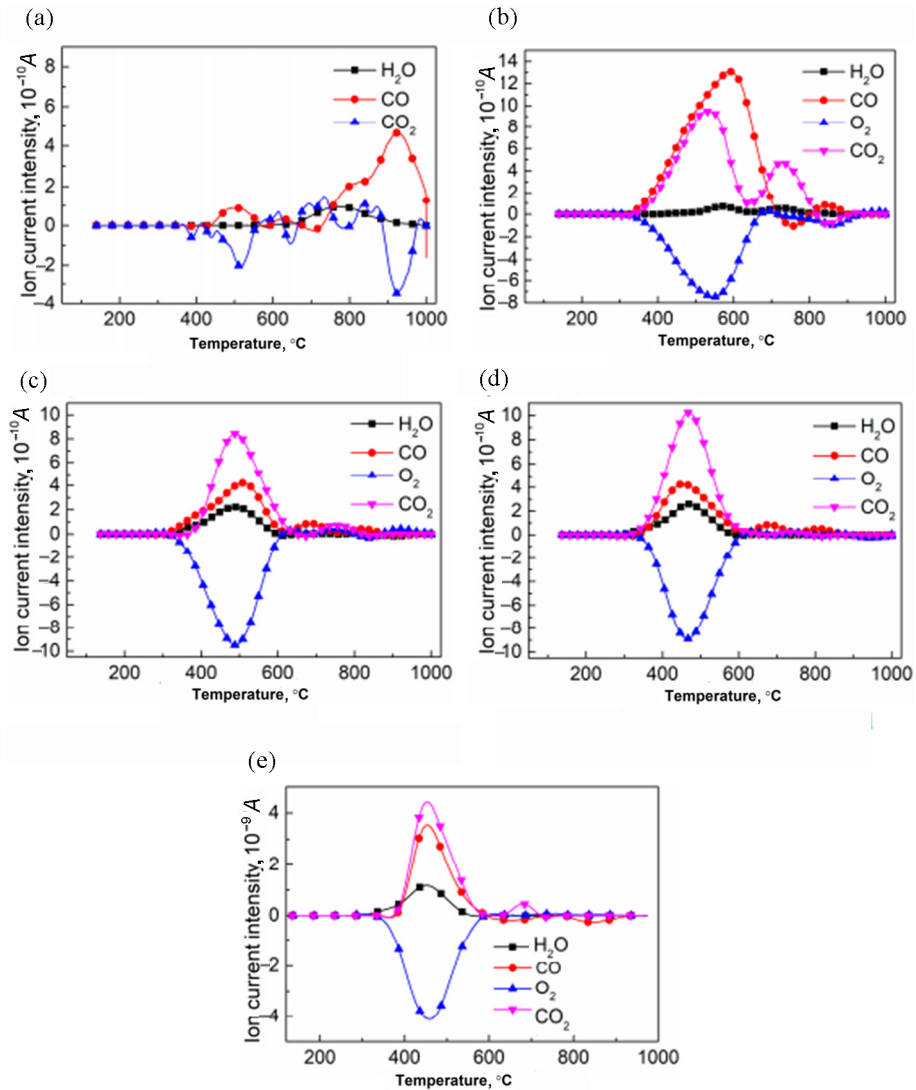


Fig. 5. Evolution of the main combustion products of sample S_3 in different atmospheres: (a) carrier gas consisting of 100% CO_2 ; (b) carrier gas consisting of 95% CO_2 and 5% O_2 ; (c) carrier gas consisting of 90% CO_2 and 10% O_2 ; (d) carrier gas consisting of 85% CO_2 and 15% O_2 ; (e) air.

sulphuration of carbonates as Reaction (7) shows, rather than to the CaO-SO_2 reaction in air as Reaction (12) reveals. As Chen et al. [32] have indicated, the formation of calcium oxide is accompanied with the decrease of BET- N_2 surface area and average pore size. So, the direct sulphuration of carbonates without formation of calcium oxide makes the sample less resistant to diffusion, and Reactions (7) and (9) occur more easily in CO_2/O_2 .

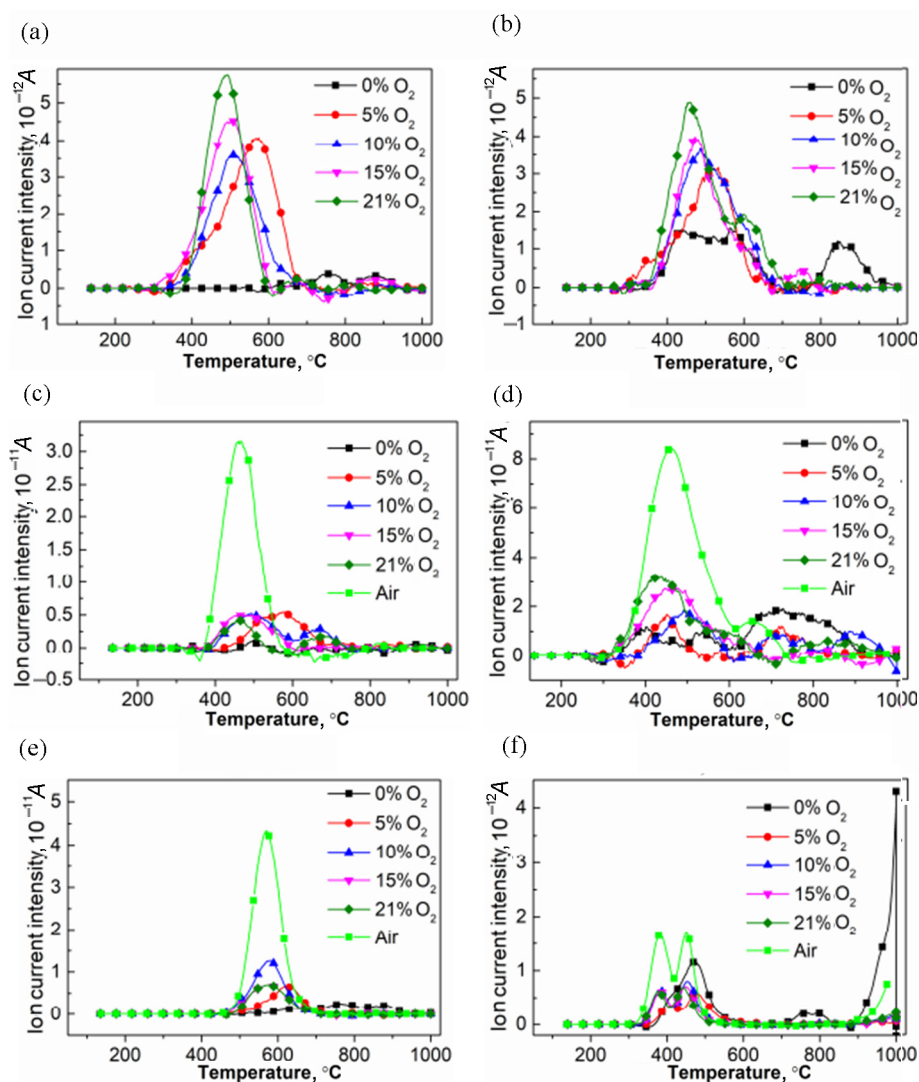


Fig. 6. Curves of hydrocarbon gas and pollutants emission in the atmosphere of O₂ of varying concentration: (a) C₂H₃; (b) C₃H₇; (c) C₂H₅; (d) NO₂; (e) NO; (f) SO₂.

That is why the activation energy of the second stage in CO₂/O₂ is lower than that in air, as seen from Table 5.



The absence of oxygen favours the decomposition of sulphates above 950 °C. At the same time, the decomposition is inhibited by increasing the

O₂ concentration, especially over 5% [33, 34]. Thus, the peak area of SO₂ during the whole oxidation process in an oxygen-bearing atmosphere is smaller than that in a pure CO₂ atmosphere. On the other hand, the peak area of SO₂ increases with increasing O₂ volume fraction of the carrier gas from 5 to 10% since increasing O₂ favors SO₂ formation. However, the SO₂ peak area shows a slight declining trend in the combustion stage when O₂ increases from 10 to 21% because abundant O₂ also facilitates SO₂ capture through Reaction (7).

4. Conclusions

This work applied thermogravimetry-mass spectrometry to investigate the combustion characteristics of the semicoke from the retorting of Huadian oil shale and wheat straw blends. The effects of the ambient atmosphere and the wheat straw fraction in matrix blends on the process were investigated. Based on the experiments and discussions, the main conclusions can be drawn as follows:

1. The basics of a new way of utilizing oil shale are introduced, involving first retorting oil shale and biomass together for oil and subsequently burning the produced semicoke blends for heat in the atmosphere of O₂/CO₂.
2. In an oxygen atmosphere, the whole oxidation process of semicoke blends consists of the combustion stage and the decomposition stage. In the combustion stage, the ignition temperatures of oil shale semicoke and wheat straw semicoke samples are quite close, so semicoke samples would ignite simultaneously rather than separately. Also, increasing the wheat straw proportion in matrix blends and elevating O₂ concentration can improve the ignition and combustion performances of the resulting semicoke. Moreover, the ignition and combustion performances of blends in 21% O₂/79% CO₂ are close to those in air. In the decomposition stage, the decomposition of carbonates is inhibited in 21% O₂/79% CO₂.
3. Compared with air, the mixture of O₂ and CO₂ is more advantageous for reducing NO_x and SO₂ emissions. Further investigation is needed to determine the optimum mixing ratio of O₂ and CO₂, in order to elucidate whether semicoke could be burnt fully and cleanly and shale oil yield increased significantly. Also, NO_x and SO₂ emissions show a declining trend with increasing wheat straw proportion in matrix samples. Furthermore, the furnace temperature at which semicoke combusts should be below 900 °C in order to inhibit SO₂ emission.

Acknowledgements

This work was supported by the National Natural Science Foundation of China (Grant No. 51876122).

REFERENCES

1. Wu, C. Z., Zhou, Z. Q., Yin, X. L., Yi, W. M. Current status of biomass energy development in China. *Transactions of the Chinese Society for Agricultural Machinery*, 2009, **40**(1), 91–99.
2. Abnisa, F., Wan Daud, W. M. A. A review on co-pyrolysis of biomass: An optional technique to obtain a high-grade pyrolysis oil. *Energ. Convers. Manage.*, 2014, **87**, 71–85.
3. Haykiri-Acma, H., Yaman, S. Interaction between biomass and different rank coals during co-pyrolysis. *Renew. Energ.*, 2010, **35**(1), 288–292.
4. Jones, J. M., Kubacki, M., Kubica, K., Ross, A. B., Williams, A. Devolatilisation characteristics of coal and biomass blends. *J. Anal. Appl. Pyrol.*, 2005, **74**(1–2), 502–511.
5. Skodras, G., Grammelis, P., Basinas, P. Pyrolysis and combustion behaviour of coal–MBM blends. *Bioresource Technol.*, 2007, **98**(1), 1–8.
6. Chen, B., Han, X., Mu, M., Jiang, X. Studies of the co-pyrolysis of oil shale and wheat straw. *Energ. Fuel.*, 2017, **31**(7), 6941–6950.
7. Cheng, X., Wang, L., Wang, Z., Zhang, M., Ma, C. Catalytic performance of NO reduction by CO over activated semi-coke supported Fe/Co catalysts. *Ind. Eng. Chem. Res.*, 2016, **55**(50), 12710–12722.
8. Ekvall, T., Andersson, K., Leffler, T., Berg, M. K–Cl–S chemistry in air and oxy-combustion atmospheres. *P. Combust. Inst.*, 2017, **36**(3), 4011–4018.
9. Yuzbasi, N. S., Selçuk, N. Air and oxy-fuel combustion characteristics of biomass/lignite blends in TGA-FTIR. *Fuel Process. Technol.*, 2011, **92**(5), 1101–1108.
10. Varol, M., Atimtay, A. T., Bay, B., Olgun, H. Investigation of co-combustion characteristics of low quality lignite coals and biomass with thermogravimetric analysis. *Thermochim. Acta*, 2010, **510**(1–2), 195–201.
11. Vamvuka, D., Tsamourgeli, V., Galetakis, M. Study on catalytic combustion of biomass mixtures with poor coals. *Combust. Sci. Technol.*, 2014, **186**(1), 68–82.
12. Gil, M. V., Casal, D., Pevida, C., Pis, J. J., Rubiera, F. Thermal behaviour and kinetics of coal/biomass blends during co-combustion. *Bioresource Technol.* 2010, **101**(14), 5601–5608.
13. Gao, Y., Tahmasebi, A., Dou, J. X., Yu, J. L. Combustion characteristics and air pollutant formation during oxy-fuel co-combustion of microalgae and lignite. *Bioresource Technol.*, 2016, **207**, 276–284.
14. Jayaraman, K., Gökalp, I. Pyrolysis, combustion and gasification characteristics of miscanthus and sewage sludge. *Energ. Convers. Manage.*, 2015, **89**, 83–91.
15. Fan, Y. L., Yu, Z. S., Fang, S. W., Lin, Y., Lin, Y. S., Liao, Y. F., Ma, X. Q. Investigation on the co-combustion of oil shale and municipal solid waste by using thermogravimetric analysis. *Energ. Convers. Manage.*, 2016, **117**, 367–374.
16. Yang, Y., Lu, X. F., Wang, Q. H. Investigation on the co-combustion of low calorific oil shale and its semi-coke by using thermogravimetric analysis. *Energ.*

- Convers. Manage.*, 2017, **136**, 99–107.
17. Han, X. X., Jiang, X. M., Cui, Z. G., Yan, J. W., Liu, J. G. Effects of retorting factors on combustion properties of shale char. *J. Therm. Anal. Calorim.*, 2011, **104**(2), 771–779.
 18. Li, X. G., Ma, B. G., Xu, L., Hu, Z. W., Wang, X. G. Thermogravimetric analysis of the co-combustion of the blends with high ash coal and waste tyres. *Thermochim. Acta*, 2006, **441**(1), 79–83.
 19. Luo, S. Y., Xiao, B., Hu, Z. Q., Liu, S. M., Guan, Y. W. Experimental study on oxygen-enriched combustion of biomass micro fuel. *Energy*, 2009, **34**(11), 1880–1884.
 20. Sahu, S. G., Sarkar, P., Chakraborty, N., Adak, A. K. Thermogravimetric assessment of combustion characteristics of blends of a coal with different biomass chars. *Fuel Process. Technol.*, 2010, **91**(3), 369–378.
 21. Coats, A. W., Redfern, J. P. Kinetic parameters from thermogravimetric data. *Nature*, 1964, **201**(4914), 68–69.
 22. Vamvuka, D., Sfakiotakis, S. Combustion behaviour of biomass fuels and their blends with lignite. *Thermochim. Acta*, 2011, **526**(1–2), 192–199.
 23. Vamvuka, D., Sfakiotakis, S., Saxioni, S. Evaluation of urban wastes as promising co-fuels for energy production – A TG/MS study. *Fuel*, 2015, **147**, 170–183.
 24. Vyazovkin, S., Chrissafis, K., Di Lorenzo, M. L., Koga, N., Pijolat, M., Roduit, B., Sbirrazzuoli, N., Suñol, J. J. ICTAC Kinetics Committee recommendations for collecting experimental thermal analysis data for kinetic computations. *Thermochim. Acta*, 2014, **590**(19), 1–23.
 25. Wall, T., Liu, Y., Spero, C., Elliott, L., Khare, S., Rathnam, R., Zeenathal, F., Moghtaderi, B., Buhre, B., Sheng, C., Gupta, R., Yamada, T., Makino, K., Yu, J. An overview on oxyfuel coal combustion – State of the art research and technology development. *Chem. Eng. Res. Des.*, 2009, **87**(8), 1003–1016.
 26. Vamvuka, D., Saxioni, S. Investigation of slagging/fouling and environmental impact of ashes produced from co-combustion of urban wastes with lignite. *Fresen. Environ. Bull.*, 2012, **21**(11), 3345–3351.
 27. Han, X., Chen, B., Li, Q., Tong, J., Jiang, X. Organic nitrogen conversion during the thermal decomposition of Huadian oil shale of China. *Oil Shale*, 2017, **34**(2), 97–109.
 28. Gai, R. H., Jin, L. J., Zhang, J. B., Wang, J. Y., Hu, H. Q. Effect of inherent and additional pyrite on the pyrolysis behavior of oil shale. *J. Anal. Appl. Pyrol.*, 2014, **105**, 342–347.
 29. Al-Makhadmeh, L. A., Maier, J., Batiha, M. A., Scheffknecht, G. Oxyfuel technology: Oil shale desulfurization behavior during staged combustion. *Fuel*, 2017, **190**, 229–236.
 30. Tian, L., Yang, W., Chen, Z., Wang, X., Yang, H., Chen, H. Sulfur behavior during coal combustion in oxy-fuel circulating fluidized bed condition by using TG-FTIR. *J. Energy Inst.*, 2016, **89**(2), 264–270.
 31. Yörüç, C. R., Meriste, T., Sener, S., Kuusik, R., Trikkel. Thermogravimetric analysis and process simulation of oxy-fuel combustion of blended fuels including oil shale, semicoke, and biomass. *Int. J. Energ. Res.*, 2018, **42**(6), 2213–2224.
 32. Chen, J., Yao, H., Zhang, P., Xiao, L., Luo, G., Xu, M. Control of PM₁ by kaolin or limestone during O₂/CO₂ pulverized coal combustion. *P. Combust. Inst.*, 2011, **33**(2), 2837–2843.

33. Yan, Z. Q., Wang, Z. A., Wang, X. F., Liu, H., Qiu, J. R. Kinetic model for calcium sulfate decomposition at high temperature. *T. Nonferr. Metal. Soc.*, 2015, **25**(10), 3490–3497.
34. Hoteit, A., Bouquet, E., Schönnenbeck, C., Gilot, P. Sulfate decomposition from circulating fluidized bed combustors bottom ash. *Chem. Eng. Sci.*, 2007, **62**(23), 6827–6835.

Presented by A. Siirde

Received February 5, 2018